Clinical and Experimental Obstetrics & Gynecology

Clin. Exp. Obstet. Gynecol. **2026**; 53(3): 48062
https://doi.org/10.31083/CEOG48062

Original Research

Sequencing Analysis Reveals Potential NAD^+-Regulated Mechanisms in Endometrial Stromal Cell Decidualization Prior to Embryo Implantation

Ming-hui Liu[1], Yao Fu[1], Shuo Han[1,*]

[1]Medical Center for Human Reproduction, Beijing Chao-Yang Hospital, Capital Medical University, 100020 Beijing, China
*Correspondence: hanshuo@mail.ccmu.edu.cn (Shuo Han)

Academic Editor: Michael H. Dahan
Submitted: 7 November 2025 Revised: 5 January 2026 Accepted: 26 January 2026 Published: 19 March 2026

Abstract

Background: This study aimed to investigate the role of nicotinamide adenine dinucleotide (NAD^+) in endometrial decidualization prior to embryo implantation and to elucidate the underlying mechanism. **Methods**: In this study, primary human endometrial stromal cells (hEnSCs) were isolated and cultured *in vitro*. Decidualization was induced under three conditions: an experimental group (EG) treated with nicotinamide mononucleotide (NMN) alongside the standard decidualization cocktail to increase intracellular NAD^+ levels; a control group (CG) that received only the standard decidualization cocktail; and a blank group (BG) that received no decidualization stimuli. Decidualization was evaluated by examining morphological changes and by measuring the secretion of specific markers, prolactin (PRL) and insulin-like growth factor binding protein-1 (IGFBP-1) using an enzyme-linked immunosorbent assay (ELISA). To explore the underlying mechanisms, transcriptomic sequencing and bioinformatics analysis were performed on cells from all three groups, followed by experimental validation. **Results**: The results indicated that increased intracellular NAD^+ enhanced endometrial decidualization, as evidenced by higher secretion of the decidual markers PRL and IGFBP-1. Transcriptomic analysis revealed significant differences between the decidualized groups (CG and EG) and the nondecidualized group (BG), which reflect major cellular reprogramming. However, transcriptomic differences between the EG and CG groups were minimal. This finding suggests that NAD^+ elevation does not initiate decidualization via broad transcriptional reprogramming but instead provides a fine-tuning, supportive effect on the already induced decidual state. Gene Set Enrichment Analysis (GSEA) indicated that NAD^+ supplementation may influence decidualization through modulating DNA replication and cell cycle pathways. In addition, NAD^+ effectively reduced apoptotic activity in decidualizing hEnSCs compared with the CG. **Conclusions**: This study establishes that increasing intracellular NAD^+ level promotes decidualization of hEnSCs. Rather than causing widespread changes in gene expression, NAD^+ appears to refine and support the decidualization process, likely through effects on DNA replication and cell cycle pathways and by reducing apoptosis. These early findings provide insight into how cellular metabolism may regulate decidualization and suggest a potential supportive role for NAD^+ modulation.

Keywords: human endometrial stromal cells; decidualization; NAD^+; embryo implantation

1. Introduction

Endometrial decidualization, which involves stromal cell differentiation into decidual cells, is essential for embryo implantation and is driven by estrogen and progesterone. This process is characterized by an epithelial-like transition, secretion of prolactin (PRL) and insulin-like growth factor binding protein-1 (IGFBP-1), as well as regulation of the cell-cycle, modulation of immune responses, and formation of new blood vessels [1,2]. Impaired decidualization causes implantation failure due to insufficient nutritional and immune support for the embryo [3]. Although luteal support therapies and immunomodulatory drugs are commonly used to enhance decidualization, 30%–40% of women with recurrent implantation failure (RIF) do not respond to these treatments [4,5], underscoring the urgent need to identify new metabolic targets for intervention.

Nicotinamide adenine dinucleotide (NAD^+), a key molecule in cellular redox balance and epigenetic regulation, modulates cell cycle regulators and antiapoptotic pathways [6,7]. In pregnant mouse models, inhibition of NAD^+ synthesis prevents decidualization and causes embryo resorption [8]. Beyond its role in stromal cell decidualization, recent research shows that NAD^+ metabolism is essential for immune homeostasis in the decidua, supporting the anti-inflammatory functions of decidual macrophages, which are vital for sustaining pregnancy [9]. Our previous study on primary human endometrial stromal cells (hEnSCs) found that patients with RIF exhibited significantly reduced oxidative phosphorylation and inactivation of peroxisome proliferator-activated receptor-gamma coactivator-1α due to hyperacetylation. This defect was reversed by supplementation with the NAD^+ precursor nicotinamide mononucleotide (NMN), which also increased PRL and IGFBP-1 expression [10]. As NAD^+ influences multiple cellular processes, understanding its specific transcriptional effects in human decidualization is essential. However, the precise regulatory network and the extent of the role of NAD^+ in hEnSCs decidualization remain unclear.

Building on these insights, this study employed an *in vitro* decidualization model of primary hEnSCs to examine how increasing intracellular NAD^+ levels via NMN supplementation affect the decidual phenotype and its underlying transcriptional program. This study proposes that NAD^+ functions primarily as a metabolic regulator rather than a direct inducer, subtly adjusting the decidualization process. By carefully comparing morphological, molecular, and transcriptomic data across controlled experimental groups, we aimed to clarify the specific roles of NAD^+ in promoting human endometrial decidualization and to elucidate the underlying mechanisms.

2. Materials and Methods

2.1 Reagents and Materials

Dulbecco's modified Eagle's medium (DMEM/F12) was purchased from Hyclone (Catalog No. SH30023.01; Shanghai, China). To eliminate potential interference from exogenous steroid hormones, all experiments used charcoal-stripped fetal bovine serum (FBS; Catalog No. 3830-0050; Vivacell, Shanghai, China; 50 mL). Conventional decidualization medium consisted of 100 nM estradiol (Catalog No. E2758; Sigma-Aldrich, Shanghai, China), 10 µM medroxyprogesterone 17-acetate (Catalog No. M1629; Sigma-Aldrich, Shanghai, China), and 50 µM 8-bromoadenosine cAMP (8-Br-cAMP; Catalog No. B7880; Sigma-Aldrich, Shanghai, China). All reagents, kits, and antibodies utilized in the present investigation are documented in the supplementary materials (**Supplementary Table 1**), including manufacturer details, product or lot numbers, and locations.

2.2 Participant Enrollment

Three donors with regular menstrual cycles were recruited at Beijing Chao-Yang Hospital, Capital Medical University from June 2020 to June 2022. Eligibility was confirmed via ultrasound and hysteroscopic examination of normal endometrial morphology. The study was approved by the hospital's ethics committee (2020-Science-279), and all participants provided written informed consent.

2.3 Isolation and Culture of hEnSCs

After obtaining informed consent, hEnSCs were isolated from endometrial biopsies collected during the late proliferative phase, defined as 5–7 days after menstruation and 3–5 days before ovulation, confirmed by ultrasound showing a dominant follicle of 14–16 mm diameter [11]. This method ensures a consistent estrogen-primed stromal environment necessary for decidualization research. Tissue collection was performed using a Pipelle® curette (Catalog No. 8200; CooperSurgical, Inc., Trumbull, CT, USA) following established protocol [10]. All tissue donors tested negative in preoperative screenings for relevant pathogens, including *Mycoplasma*, Hepatitis B virus, Hepatitis C virus, human immunodeficiency virus, and *Treponema pallidum*. For cell isolation and culture, endometrial tissues were washed twice, minced into 1–2 mm fragments, and then dissociated with 0.25% trypsin–ethylenediaminetetraacetic acid (0.53 mM) at 37 °C for 30 min. The resulting cell suspension was then filtered using a sterile 100 µm cell strainer. The endometrial cells were suspended in DMEM/F12 medium with 2% charcoal-stripped FBS. Cells were plated onto standard culture plates. Cell identity was confirmed by characteristic spindle-shaped morphology and immunofluorescence: positive staining for the mesenchymal markers vimentin (Catalog No. ab92547; Abcam, Cambridge, UK) and CD90 (Catalog No. 555595; BD Biosciences, San Jose, CA, USA), and negative staining for the epithelial marker cytokeratin 18 (CK18; Catalog No. ab668; Abcam, Cambridge, UK) (**Supplementary Fig. 1**). The cells were used at low passage numbers (passages 2–4) for all subsequent experiments.

2.4 Experimental Grouping and Morphological Assessment

Primary hEnSCs were assigned into three experimental groups, as presented in Fig. 1: the blank group (BG), in which cells were cultured in standard medium without decidualization-inducing agents; the control group (CG), cultured in standard decidualization induction medium; and the experimental group (EG), cultured in the same induction medium but supplemented with 200 µM NMN. Cells from each group were seeded on poly-L-lysine–coated 35-mm dishes in DMEM/F12 containing 10% FBS and then allowed to adhere for 24 h. Morphological changes were monitored, and images were captured using a phase-contrast microscope (Olympus, Tokyo, Japan) equipped with a complementary metal-oxide-semiconductor (CMOS) digital camera (Model No. DP74; Olympus Corporation, Tokyo, Japan).

2.5 RNA Sequencing (RNA-seq) and Data Analysis

Culture medium was changed every 48 hours for all groups to ensure consistent conditions. Following a 6-day culture, hEnSCs were collected, snap-frozen in liquid nitrogen, and stored for RNA extraction. Total RNA isolation was performed using the RNeasy Plus Mini Kit (Catalog No. 74134; Qiagen, Hilden, Germany) according to the manufacturer's instructions. RNA purity and concentration were quantified on a Qubit® 2.0 Fluorometer (Catalog No. Q32866; Thermo Fisher Scientific, Waltham, MA, USA) with the Qubit® RNA Assay Kit (Catalog No. Q32852; Thermo Fisher Scientific, Waltham, MA, USA) following the manufacturer's instructions. RNA integrity was assessed using an Agilent Bioanalyzer 2100 system (Software Version B.02.09; Agilent Technologies, Santa Clara, CA, USA). For each sample, RNA-seq libraries were constructed from 3 µg of total RNA using the TruSeq RNA Library Prep Kit v2 (Catalog No. RS-122-2001; Illumina, San Diego, CA, USA). cDNA fragmentation and fragment purification were conducted following standard procedures.

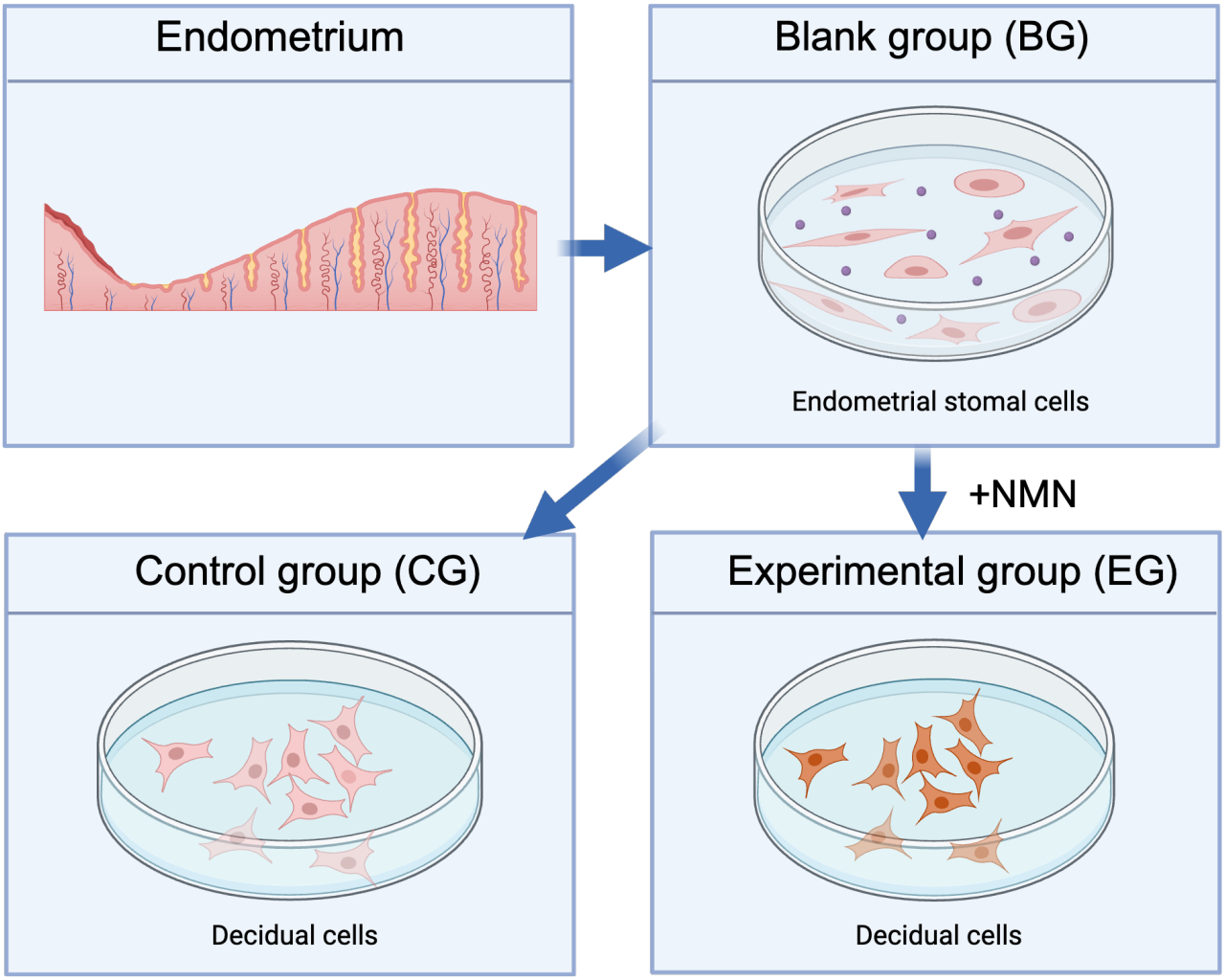

Fig. 1. Experimental workflow for hEnSC treatment. After endometrial tissue collection, samples were processed *in vitro* to establish primary hEnSC cultures. The BG received no decidualization stimulus, the CG was treated with the conventional decidualization protocol, and the EG received the same protocol supplemented with NMN. hEnSC, human endometrial stromal cells; BG, blank group; CG, control group; EG, experimental group; NMN, nicotinamide mononucleotide.

Sequencing was conducted on the Illumina NovaSeq 6000 platform (Illumina, San Diego, CA, USA). This approach yielded an average of approximately 6 gigabytes (Gb) of data for each sample.

Raw paired-end RNA-seq reads were quality-checked and trimmed for adapters using Trimmomatic (v0.39; Usadel Lab, Aachen, Germany). Cleaned reads were aligned against the GRCh38 reference genome with HISAT2 (v2.0.5; Johns Hopkins University, Baltimore, MD, USA) and subsequently assembled using StringTie (v2.1.4; Johns Hopkins University, Baltimore, MD, USA). FeatureCounts (v2.0.1; Walter and Eliza Hall Institute, Melbourne, Australia) was used to quantify reads for each gene annotated using Ensembl v98 (European Bioinformatics Institute, Cambridge, UK). Gene expression was expressed as raw read counts and then normalized to fragments per kilobase of transcript per million mapped reads (FPKM) for visualization, such as heatmaps or sample clustering [12].

Differential expression analysis was performed with DESeq2 (v1.34.0; Bioconductor, Buffalo, NY, USA) [13], using criteria of an adjusted p-value of <0.05 (Benjamini–Hochberg correction) and an absolute fold change of >1.5. Gene Ontology (GO) and Kyoto Encyclopedia of Genes and Genomes (KEGG) pathway enrichment analyses of the differentially expressed genes (DEGs) were performed using custom Python scripts (v3.8; Python Software Foundation, Wilmington, DE, USA). Gene Set Enrichment Analysis (GSEA; v4.1.0; Broad Institute, Cambridge, MA, USA) was employed with gene sets obtained from the MSigDB database (MSigDB; Broad Institute, Cambridge, MA, USA). The complete list of gene sets used is provided in **Supplementary Table 2**. Gene signatures are supplied upon request. Statistical significance was set at a false discovery rate (FDR) <0.25 and $p < 0.05$.

2.6 Quantitative Real-Time Polymerase Chain Reaction (qRT-PCR)

As instructed by the manufacturer, total RNA was isolated using the TRIzol® Plus RNA Purification Kit (Catalog No. 12183555; Thermo Fisher, Carlsbad, CA, USA). Complementary DNA (cDNA) was synthesized using the SuperScript™ III First-Strand Synthesis SuperMix (Catalog No. 11752250; Thermo Fisher, Carlsbad, CA, USA). qRT-PCR was performed using PowerUp™ SYBR™ Green Master Mix (Catalog No. A25742; Applied Biosystems, Carlsbad, CA, USA) following the manufacturer's guidelines. The qRT-PCR cycling program comprised an initial denaturation step at 95 °C for 2 min, followed by 40 amplification cycles. Target gene expression was normalized to β-actin and analyzed using the $2^{-\Delta\Delta Ct}$ method [14]. Results are presented as fold change relative to the mean of the control group. The corresponding primer sequences are detailed in the supplementary materials (**Supplementary Table 3**).

2.7 Western Blot (WB)

Protein extraction from hEnSCs in each group was performed using radioimmunoprecipitation (RIPA) assay buffer (Catalog No. 89900; Thermo Fisher Scientific, Waltham, MA, USA) supplemented with added protease and phosphatase inhibitors (Catalog No. 78440; Thermo Fisher Scientific, Waltham, MA, USA). Protein concentration was determined with a bicinchoninic acid assay kit (Catalog No. P0012S; Beyotime Biotechnology, Shanghai, China). For each sample, 30–50 µg of total protein was separated by SDS-PAGE and transferred to a polyvinylidene fluoride (PVDF) membrane (Hybond-P; Catalog No. 10600023; GE Healthcare, Chicago, IL, USA) via wet transfer. Following a 1-hour block at room temperature in Tris-buffered saline with 0.1% Tween-20 (TBST), the membranes were incubated overnight at 4 °C with primary antibodies diluted in the same blocking buffer. After thorough washing with TBST, the membranes were incubated with horseradish peroxidase-conjugated goat anti-rabbit secondary antibody (1:5000; Catalog No. 31460; Thermo Fisher Scientific, Waltham, MA, USA) for 1 h at room temperature. Protein bands were visualized using the SuperSignal West Dura Extended Duration Chemiluminescent Substrate (Catalog No. 34075; Thermo Fisher Scientific, Waltham, MA, USA) and detected on X-ray film or with a digital imaging system. Band intensities were quantified with Image Pro Plus 6.0 software (v6.0; Media Cybernetics, Rockville, MD, USA). For total proteins, such as IGF2BP2, GSS, and POLD1, expression levels were normalized to β-actin. For phosphorylated Akt and cleaved Caspase-9, signals were normalized to total Akt and total Caspase-9 levels, respectively.

2.8 Statistical Analysis

The clinical characteristics of tissue donors are summarized in **Supplementary Table 4**. Before analysis, data normality was assessed with the Shapiro–Wilk test, and homogeneity of variance was confirmed using Levene's test. Comparisons between groups used an unpaired two-tailed Student's *t*-test. For three or more groups, one-way analysis of variance (ANOVA) was performed, followed by Tukey's honestly significant difference (HSD) test for post-hoc comparisons when the ANOVA result was significant. All statistical analyses were conducted with GraphPad Prism (v9.5; GraphPad Software, Boston, MA, USA) or R (v4.2.2; R Foundation for Statistical Computing, Vienna, Austria). A p-value of <0.05 was considered statistically significant.

3. Results

3.1 NAD^+ Enhances the Decidualization of hEnSCs

To determine the optimal NMN concentration, the NAD^+/NADH redox ratio was measured in endometrium cells treated with 0-500 µM NMN (**Supplementary Table 5**). Treatment with 200 µM NMN led to a consistent two-fold increase in the ratio without causing cytotoxicity and was used for all subsequent experiments (Fig. 2a). By day 6, hEnSCs in both the CG and EG demonstrated typical morphological changes, transitioning from slender, spindle-shaped fibroblasts to round, polygonal cells, whereas cells in the BG retained their fibroblastic morphology (Fig. 2b and **Supplementary Fig. 2**). Immunofluorescence staining for F-actin confirmed this shift: after decidualization, the cells became rounded, exhibiting a "cobblestone" appearance and prominent peripheral actin rings, unlike the elongated stress fibers observed in nondecidualized cells (Fig. 2c). The secretion of the decidual markers PRL and IGFBP-1, measured using enzyme-linked immunosorbent assay (ELISA), was significantly higher in both the CG and EG compared with BG, with the EG displaying the highest level (Fig. 2d). These findings indicate that increasing intracellular NAD^+ by NMN supplementation enhances the morphological and functional changes associated with decidualization in hEnSCs.

3.2 Elevated NAD^+ Levels Induce Minimal Transcriptional Divergence During Decidualization

To evaluate the global transcriptional effects of NAD^+ supplementation, RNA-seq was performed on hEnSCs from the three experimental groups. Unsupervised analysis showed that the two decidualized groups (CG and EG) clustered together and were clearly distinct from the nondecidualized group (BG), as shown by hierarchical clustering of all expressed genes (Fig. 3a) and principal component analysis (Fig. 3b). This pattern was supported by the number of DEGs, with the fewest identified in the direct comparison between CG and EG (Fig. 3c, **Supplementary Table 6**). A targeted heatmap of these DEGs highlighted their limited number and consistent expression trends (Fig. 3d). In agreement with their higher transcriptional activity, KEGG pathway analysis of BG vs. CG and BG vs. EG compar-

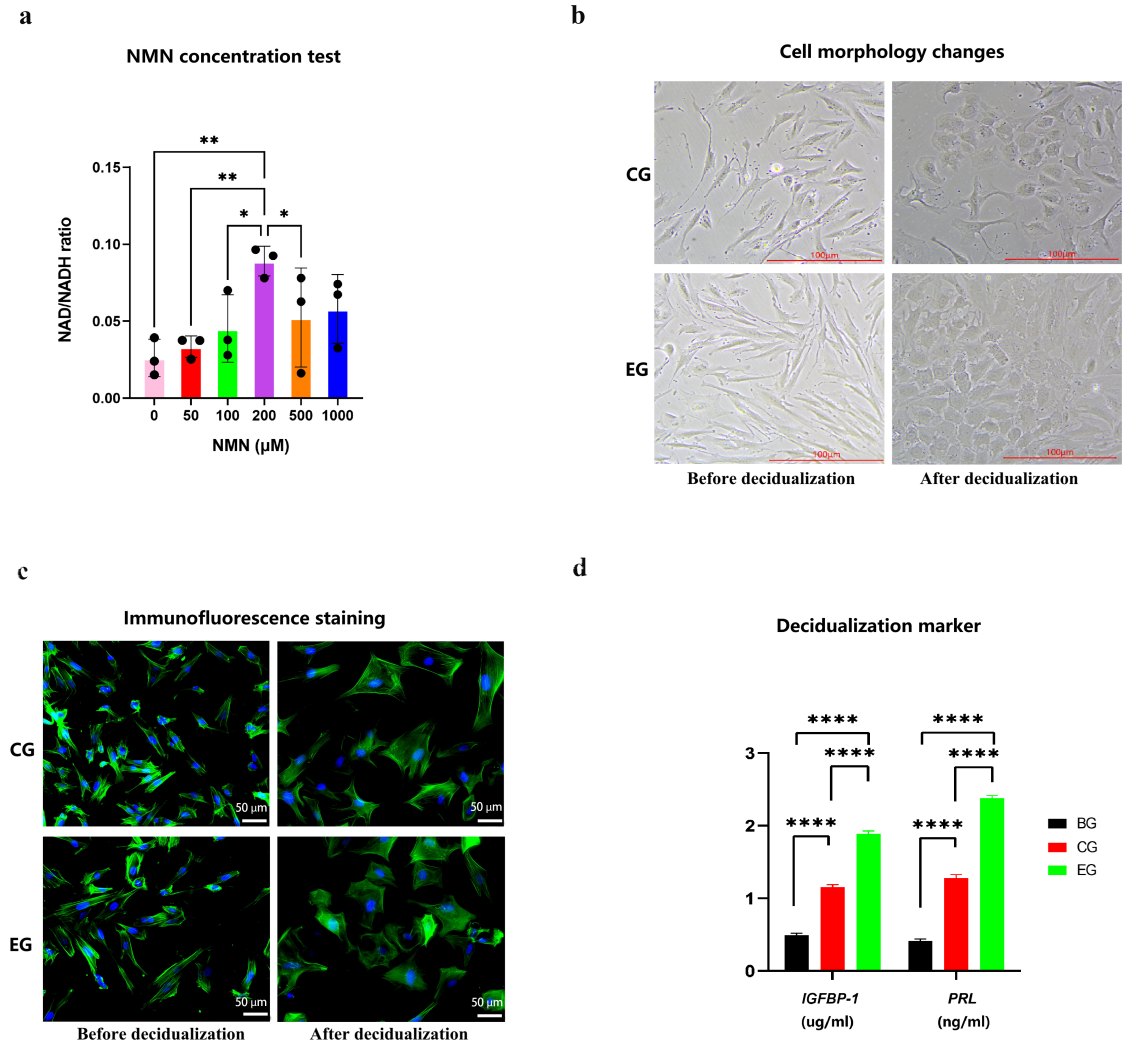

Fig. 2. Effects of NAD$^+$ on decidualization of hEnSCs. (a) Optimization of NMN concentration. The NAD$^+$/NADH ratio reached its maximum at 200 μM NMN. (b) Morphological transformations during decidualization. Cells in both the CG and EG showed characteristic decidual change. Before induction, hEnSCs presented fibroblast-like spindle shapes with elongated cell bodies and processes, organized in parallel or swirling bundles. After induction, the cells underwent an epithelioid transition, adopting a rounded, polygonal, or cobblestone-like morphology, accompanied by marked increase in cell volume and cytoplasmic content, scale bar = 100 μm. (c) F-actin and nuclear staining. Representative immunofluorescence images of hEnSCs labeled for F-actin (phalloidin-Alexa Fluor 488, green) and nuclei (DAPI, blue). Before decidualization, cells in the CG and EG displayed spindle-shaped morphology with elongated stress fibers. Following decidualization, cells acquired a rounded, polygonal cobblestone-like appearance, accompanied by increased cell size and prominent peripheral actin rings. Nuclear morphology also changed from elongated/oval to large and round. Scale bar = 50 μm. (d) Secretion of decidual markers. Concentrations of PRL and IGFBP-1 in the culture supernatant were measured by ELISA after 6 days of treatment. Compared with the BG, the secretion levels of both PRL and IGFBP-1 were significantly elevated in the CG and EG. Furthermore, the EG demonstrated significantly higher secretion of both markers than the CG. (*$p < 0.05$, **$p < 0.01$, ****$p < 0.0001$). PRL, prolactin; IGFBP-1, insulin-like growth factor binding protein-1; ELISA, enzyme-linked immunosorbent assay.

isons revealed only one commonly upregulated pathway (ko03110: chaperones and folding catalysts; **Supplementary Tables 7,8**). Interestingly, DNA replication and cell cycle pathways (ko04110 and ko03032) were selectively downregulated in the EG compared with the BG. No pathway achieved statistical significance in the CG vs. EG comparison, emphasizing the subtle nature of NAD$^+$-induced transcriptional changes. Therefore, within the context of this study, increasing NAD$^+$ does not activate a separate transcriptional program but produces a profile closely resembling that induced by standard hormonal stimuli. The selective downregulation of replication and cell cycle genes in EG may signify a refined regulation of the decidualization process, warranting further research.

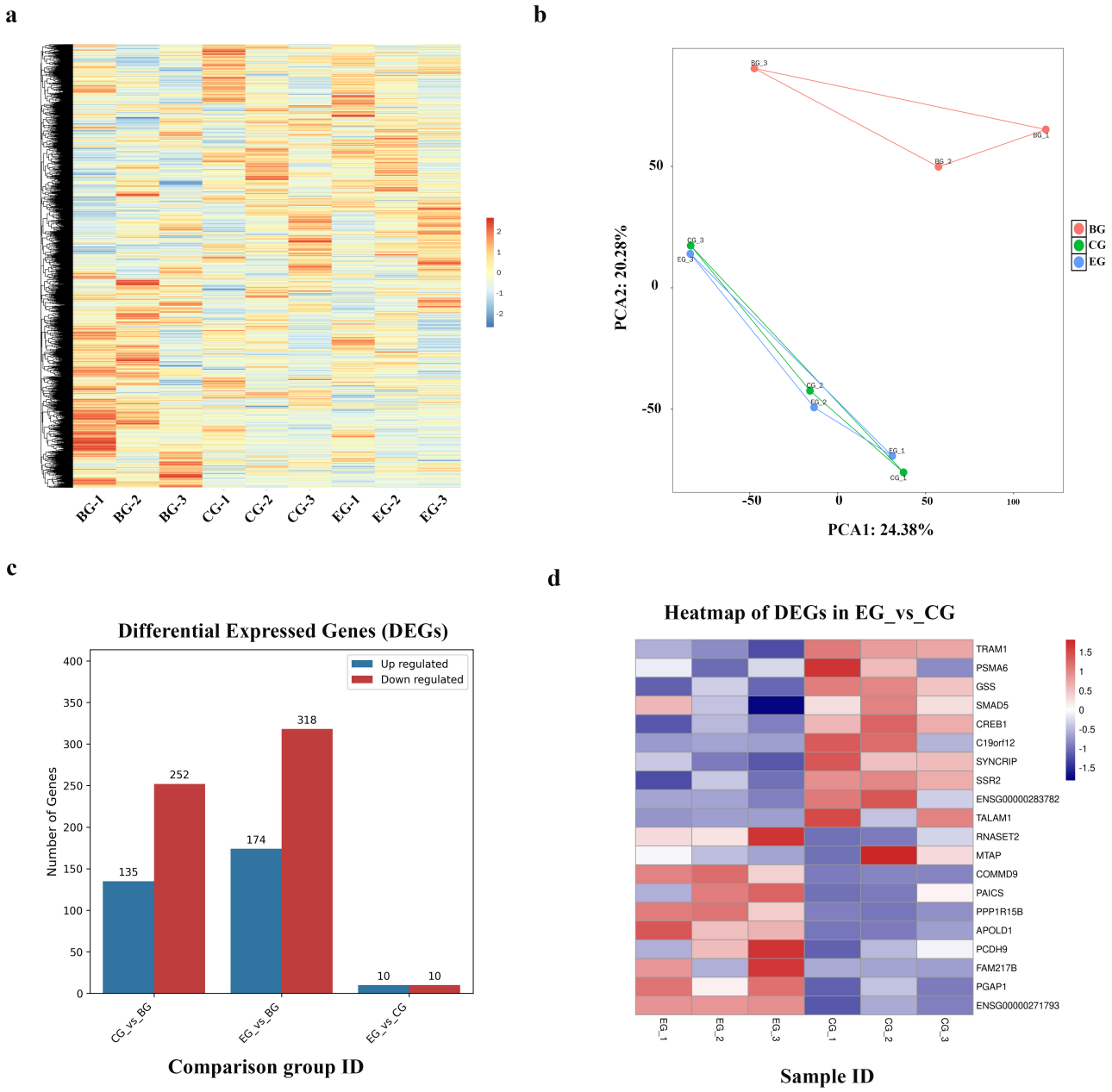

Fig. 3. Overview of gene expression patterns across the three treatment groups. (a) The heatmap of all identified genes for the three treatment groups. (b) PCA plot of all samples from the three treatment groups. (c) Differentially expressed genes (DEGs) between different groups. (d) Heatmap of DEGs in EG vs CG.

3.3 GSEA Suggests DNA Replication, Cell Cycle, and RNA-Binding Footprints of NAD$^+$

GSEA was performed to identify subtle transcriptional differences between EG and CG. All significant gene sets were enriched in the CG and, therefore, downregulated in EG (Table 1). The top-ranking categories included "DNA replication" (Fig. 4a; **Supplementary Tables 9,10**) and gene sets associated with "IGF2BP2 binding" (Fig. 4b; **Supplementary Tables 9,11**). Core genes within the DNA replication module, such as *POLD1*, *POLD2*, and *MCM7*, were consistently downregulated in the EG (Fig. 4a). Considering the established role of IGF2BP2 in stabilizing m6A-modified transcripts, NAD$^+$ was hypothesized to modulate the expression of its potential targets. Reverse transcription quantitative polymerase chain reaction (RT-qPCR) analysis confirmed that mRNA levels of *IGF2BP2*, *GSS*, and *POLD1* were significantly lower in the EG than in both CG and BG (Fig. 4c). At the protein level, WB analysis confirmed the significant downregulation of IGF2BP2 and GSS, whereas POLD1 exhibited a consistent but nonsignificant decreasing trend (Fig. 4d). To explore a potential epitranscriptomic mechanism, *in silico* analysis was performed using the m6A-Atlas database [15]. This analysis predicted multiple putative m6A modification

Table 1. Overview of the gene sets identified by GSEA that were significantly enriched in the EG compared with the CG.

Comparison_ID	Dataset shortname	Sub-dataset name	Regulation	Enriched_pathway_No. (NOM p-val < 0.01, FDR q-val <0.25)	Upregulated gene percentage	Downregulated gene percentage
EG_vs_CG	C2		down	27	48.90%	51.10%
EG_vs_CG	C2		up	0	48.90%	51.10%
EG_vs_CG	C3	Transcription factors	down	1	48.90%	51.10%
EG_vs_CG	C3	microRNA	down	1	48.90%	51.10%
EG_vs_CG	C3	Transcription factors	up	0	48.90%	51.10%
EG_vs_CG	C3	microRNA	up	0	48.90%	51.10%
EG_vs_CG	C5		down	7	48.90%	51.10%
EG_vs_CG	C5		up	0	48.90%	51.10%
EG_vs_CG	C8		down	0	48.90%	51.10%
EG_vs_CG	C8		up	0	48.90%	51.10%

val, value; FDR, false discovery rate; GSEA, Gene Set Enrichment Analysis.

Table 2. Predicted m6A modification sites within key regulators of genome replication and apoptosis.

Genesymbol	Chr_No.	Chr_start	Chr_end	Strand	Position_type	m6A_site_sequence
POLD1	chr19	50886474	50886474	+	upstream;downstream other	CCTCAGGGTCACCTCCCTGGACAAGGTGAATCAGAACTCAC
POLD1	chr19	50902218	50902218	+	exonic protein_coding	GCCATCCCAATTCGAGGAGGACCTGGCACTGATGGAGGAGA
POLD1	chr19	50902688	50902688	+	exonic protein_coding	GCCCACACCACCAGCGCTGGACCCCCAGACAGAGCCCCTCA
POLD1	chr19	50902696	50902696	+	exonic protein_coding	CACCAGCGCTGGACCCCCAGACAGAGCCCCTCATCTTCCAA
POLD1	chr19	50906811	50906811	+	exonic protein_coding	CACCGGTTACAACATCCAGAACTTCGACCTTCCGTACCTCA
POLD1	chr19	50906846	50906846	+	exonic protein_coding	ACCTCATCTCTCGGGCCCAGACCCTCAAGGTGAGGGCTGGG
POLD1	chr19	50909445	50909445	+	exonic protein_coding	CCTCTCCTCCTCAGGTACAAACATTCCCTTTCCTGGGCCGT
POLD1	chr19	50919497	50919497	+	intronic other	ACAGACTCTGTGGCCCAGAGACTCCGTGACCTCCGACCCCA
POLD1	chr19	50921180	50921180	+	exonic protein_coding	CAGCTCCTGCGGCGCTTCGGACCCCCTGGACCTGAGGCCTG
POLD1	chr19	50921189	50921189	+	exonic protein_coding	CGGCGCTTCGGACCCCCTGGACCTGAGGCCTGGTGACCTTG
GSS	chr20	33516316	33516316	-	UTR3 protein_coding	AGTGCCTGACTTGGGATAGGACTGAGTGGTAGGAGGAGGGG
GSS	chr20	33516328	33516328	-	UTR3 protein_coding	TCAGCAGGTTCCAGTGCCTGACTTGGGATAGGACTGAGTGG
GSS	chr20	33516731	33516731	-	exonic protein_coding	GGAAAAGACACTCGTGATGAACAAGCACGTGGGGCATCTAC
GSS	chr20	33516880	33516880	-	intronic protein_coding	GACTCCAGAGAGGCATAGAGACTCTAAAATCCTAGCACTTT
GSS	chr20	33516932	33516932	-	intronic protein_coding	TAGCACCAAGAGGACTCAGAACACATGGTTTGACAACCTAG
GSS	chr20	33517342	33517342	-	exonic protein_coding	GGCCCTGAAACAGCTGAAGGACAGTGAGGAGAGGGCCTCCT
GSS	chr20	33517353	33517353	-	exonic protein_coding	GAAATGGTACAGGCCCTGAAACAGCTGAAGGACAGTGAGGA
GSS	chr20	33519884	33519884	-	exonic protein_coding	ACATGCTGCCAAGTGCCCAGACATTGCCACCCAGCTGGCTG
GSS	chr20	33524621	33524621	-	exonic protein_coding	ACATCCATGTGATCCGACGAACATTTGAAGATATCTCTGAA
GSS	chr20	33529563	33529563	-	exonic protein_coding	TCTAATAATCCCAGCAAGGGACTGGCCCTGGGAATTGCCAA
GSS	chr20	33529632	33529632	-	exonic protein_coding	AGCCATCTCTCTTCCAACAGACATGTTCTCAGTGTCCTGAG

UTR3, 3'-untranslated region.

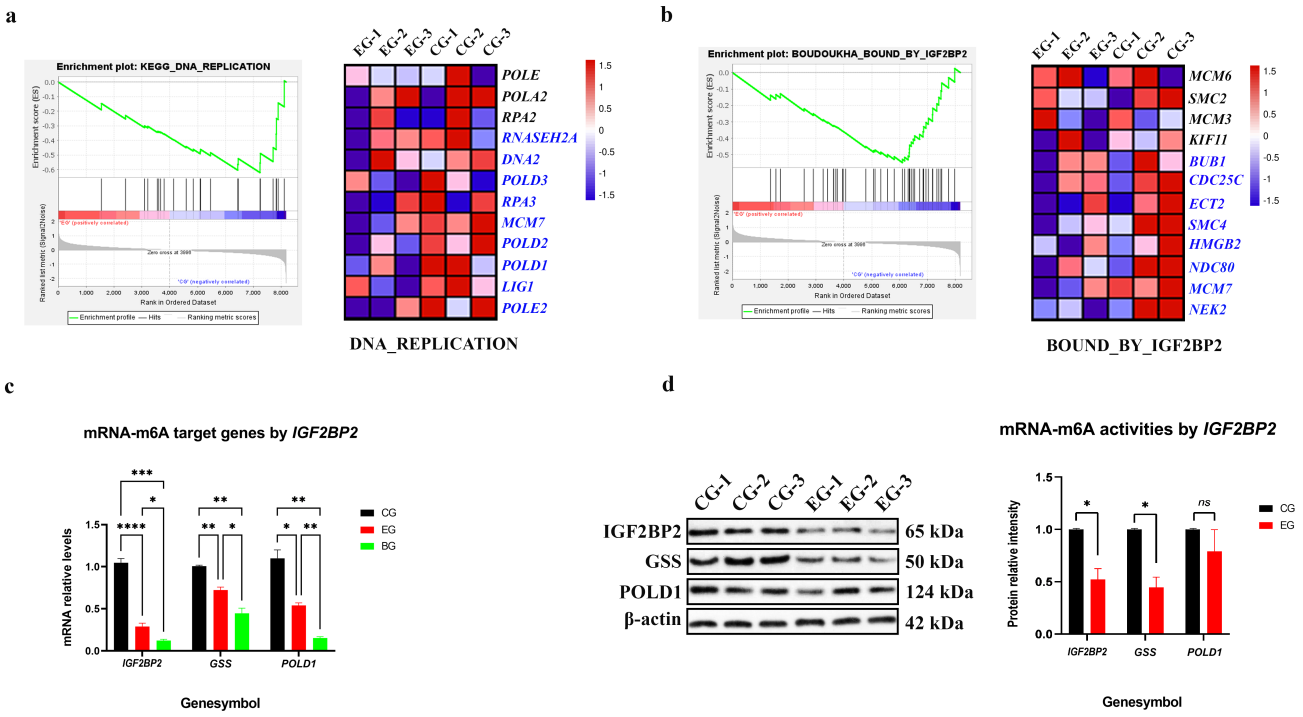

Fig. 4. GSEA identifies downregulated pathways in the EG group and validation of candidate targets. (a) Enrichment of the DNA replication pathway. (Left) GSEA enrichment plot for the "DNA replication" pathway in EG vs. CG. (Right) Heatmap of core-enriched genes from this pathway; red indicates higher expression in the CG. (b) Enrichment of IGF2BP2-binding gene set. (Left) GSEA enrichment plot. (Right) Heatmap of core-enriched genes from this set; red indicates higher expression in the CG. (c) mRNA expression of candidate targets. Relative mRNA levels of IGF2BP2, GSS, and POLD1 in BG, CG, and EG groups, measured by qPCR. Data are normalized to β-actin and presented as mean $\pm$ SD. (d) Protein expression of candidate targets. Representative WBs (performed in triplicate) are shown with β-actin as the loading control. Bar graphs display quantified protein levels (mean $\pm$ SD). (*$p < 0.05$, **$p < 0.01$, *** $p < 0.001$, **** $p < 0.0001$, *ns*, not significant). qPCR, quantitative polymerase chain reaction; SD, standard deviation; WB, western blot.

sites within the transcripts of *GSS* (10 sites) and *POLD1* (11 sites), compared with only two sites in the control gene *BAD* (Table 2). Together, these data supports a model in which increased NAD^+ levels correlate with the suppression of specific genes, some of which are predicted m6A targets, potentially implicating an IGF2BP2-related pathway. However, this link remains speculative and requires direct experimental validation.

3.4 NAD^+ Attenuates Apoptosis-Related Signaling in Decidualized hEnSCs

Significant downregulation of the Akt phosphorylates targets in the cytosol pathway in the EG (versus CG) was identified through GSEA against the Reactome database (normalized enrichment score = –1.83; Fig. 5a and **Supplementary Table 9**). Core genes within this set included *AKT1S1*, *CASP9*, and the proapoptotic factor *BAD*, implying a potential suppression of apoptotic signaling by NAD^+. Advanced analysis further corroborated this conclusion by revealing a coordinated suppression of genes involved in cell cycle and apoptosis pathways in the EG (**Supplementary Fig. 3**). A heatmap of genes from the cell cycle gene set visually supported this finding, showing higher expression (red) mainly in the CG (Fig. 5b). To confirm these transcriptional changes functionally, the activation state of key apoptotic mediators was assessed. WB analysis revealed that phosphorylated Akt (Ser473) and the cleaved (active) Caspase-9 fragment levels were significantly lower in the EG than in CG (Fig. 5c). Quantitative analysis of p-Akt/total Akt and cleaved Caspase-9/total Caspase-9 ratios indicated that both Akt kinase activity and Caspase-9 proteolytic activation were reduced at higher NAD^+ level (Fig. 5d). These findings suggest that NAD^+ supplementation suppresses the proapoptotic Akt signaling pathway at both the transcriptional and protein functional levels during decidualization.

4. Discussion

This study revealed that increasing intracellular NAD^+ level improves the decidualization capacity of primary hEnSCs without inducing widespread changes in gene expression. Building on earlier research linking NAD^+ metabolism to endometrial receptivity [6–8], these findings demonstrated a "fine-tuning" effect, in which NAD^+ supplementation strengthens an already initiated decidual

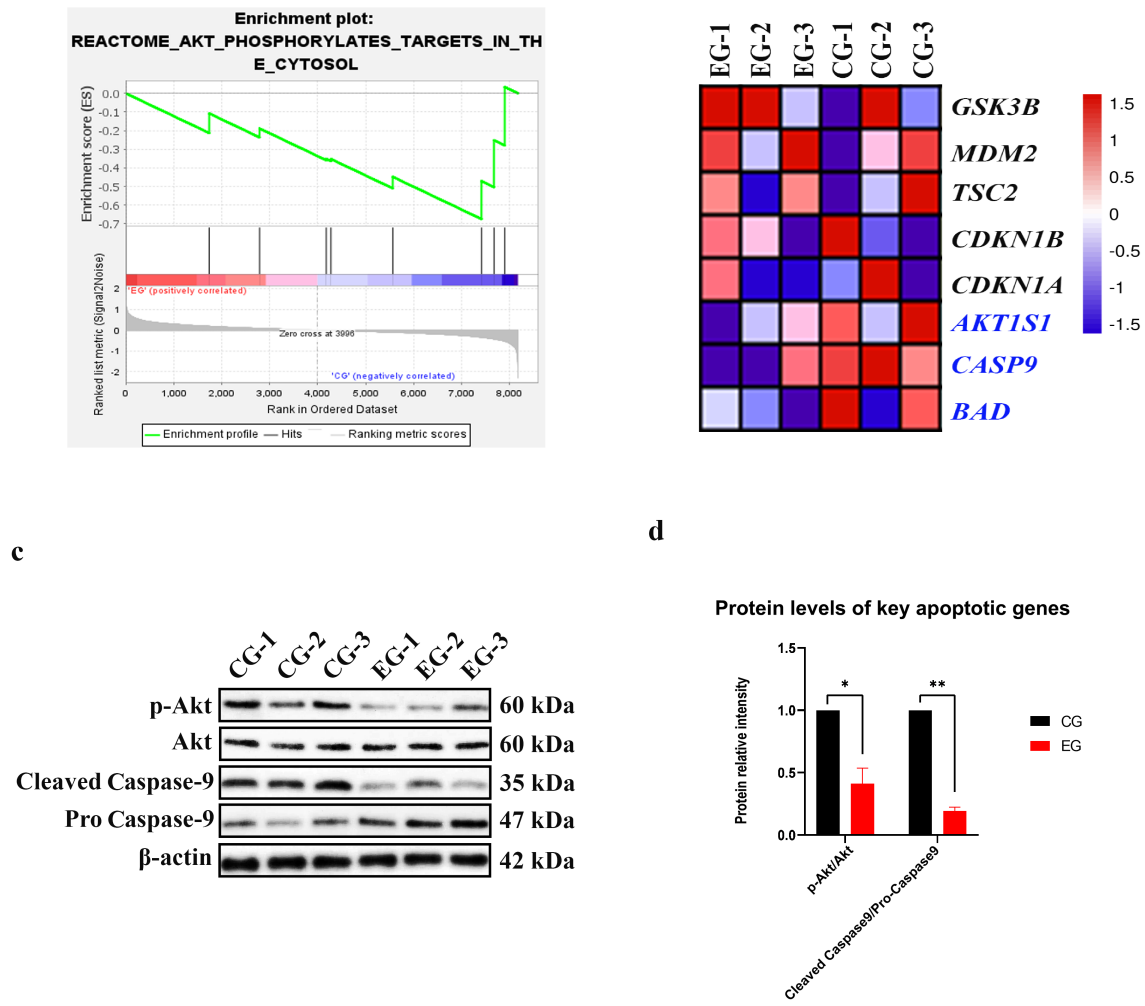

Fig. 5. GSEA identifies the downregulation of Akt signaling in the EG group, confirmed at the protein level. (a) GSEA enrichment plots in the EG vs. CG. (b) Heatmap of genes labeled in the cell cycle gene set, with red indicating higher expression in the CG. (c) Protein expression analysis of Akt and CASP9. Representative blots for phosphorylated Akt (Ser473, pAkt), total Akt, cleaved Caspase-9, total Caspase-9, and loading control β-actin are shown (performed in triplicate). (d) Bar graphs show the quantitative ratios of p-Akt/total Akt and cleaved Caspase-9/total Caspase-9, representing relative kinase and protease activity. Data are presented as mean $\pm$ SD; *$p < 0.05$, **$p < 0.01$.

process. This process is characterized by increased secretion of classical markers PRL and IGFBP-1 [1,16], reduced proapoptotic signaling [7,8], and minimal transcriptional alterations.

A key observation is the stark difference between the marked functional improvement and the minimal transcriptomic variations observed between the NAD^+-supplemented group (EG) and the standard stimulation group (CG). Both groups reached the same early decidual stage, as evidenced by their shared early decidual gene signatures (Fig. 2b) [17]. This observation indicates that NAD^+ does not accelerate developmental progression but rather boosts functional performance within the same stage. This intra-stage enhancement is supported by three key points: (1) increased secretion of markers accompanied by reduced apoptotic signals; (2) high overall transcriptional similarity and few gene expression differences between the EG and CG (Fig. 3 and **Supplementary Table 5**); and (3) pathway-level modifications, including the downregulation of DNA replication and cell cycle modules (e.g., *POLD1* and *MCM7*) [18,19], possibly reflecting a more complete exit from proliferation, which is essential for stable decidualization.

The unbiased transcriptomic analysis performed in this study mechanistically identified the RNA-binding protein IGF2BP2 as a candidate for further investigation. GSEA revealed a downregulation of gene sets associated with IGF2BP2 binding activity in the EG group (Fig. 3a,c).

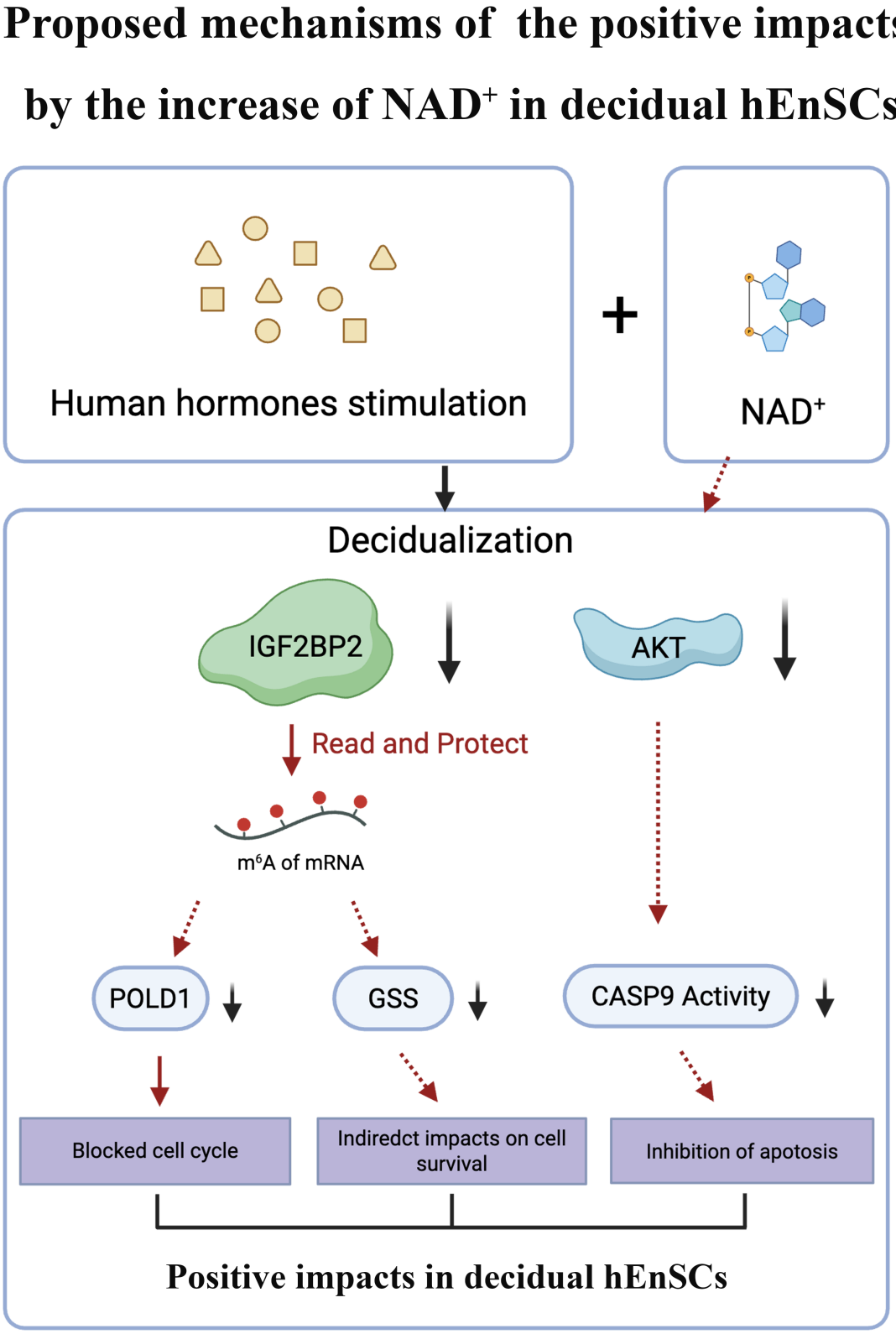

Fig. 6. Proposed model illustrating the effect of NAD^+ on decidualization.

Moreover, IGF2BP2 expression, along with its potential targets GSS and POLD1, was decreased at both mRNA and protein levels (Fig. 4). *In silico* analysis also predicted several m6A modification sites within these transcripts (Table 2) [20]. It should be emphasized that these findings are correlational and serve to generate testable hypotheses. Our study did not directly validate m6A methylation, RNA binding, or the functional role of IGF2BP2. Conse-

quently, the proposed IGF2BP2-m6A axis remains a plausible but unconfirmed model by which NAD^+ could regulate mRNA stability, pending validation using approaches such as m6A-RIP, RNA immunoprecipitation, or loss-of-function experiments. Furthermore, NAD^+ supplementation was associated with reduced proapoptotic signaling, as inferred from decreased Akt phosphorylation and lower levels of cleaved Caspase-9 (Fig. 5). This observation supports the established role of NAD^+-dependent sirtuins in promoting cell survival [7,8] and suggests a model in which NAD^+ improves decidual cell health by modulating gene expression and supporting survival (Fig. 6).

Limitations

This study has several limitations that highlight its preliminary status. First, the analysis is based on a single early time point (6 days). Longitudinal sampling is necessary to determine whether the fine-tuning effects persist or change over time. Second, the study involves a relatively small sample size. Although three independent experiments were conducted to improve reliability, a larger sample size would yield greater statistical power and stronger evidence for the findings. Lastly, while the *in vitro* model was well-controlled, it may not fully capture the multifaceted paracrine-immune cross-talk of the decidua *in vivo*.

5. Conclusions

In summary, our results support a model in which NAD^+ functions as a metabolic regulator of human endometrial decidualization. It enhances functional performance and cell survival without triggering a specific transcriptional program, possibly by influencing pathways such as cell cycle exit and RNA metabolism. Although the precise mechanisms, particularly the role of IGF2BP2, require further investigation, this research emphasizes the therapeutic potential of targeting NAD^+ metabolism to enhance endometrial receptivity. Future research involving functional validation, multi-omics time courses, and *in vivo* models will be crucial for translating these mechanistic insights into clinical strategies for patients with implantation challenges.

Availability of Data and Materials

The raw sequence data from this study have been deposited in the publicly accessible NCBI Sequence Read Archive (SRA) database as BioProject number, PRJNA1279372 and accession number SAMN49479605-SAMN49479613. The datasets supporting the conclusions of this article are included within the article and its additional files. The datasets used or analyzed during the current study are available from the authors on reasonable request.

Author Contributions

ML and SH: Conceptualization, Methodology. ML: Formal analysis, Writing-Original draft preparation. YF: Data curation, Investigation. SH: Resources. All authors contributed to editorial changes in the manuscript. All authors read and approved the final manuscript. All authors have participated sufficiently in the work and agreed to be accountable for all aspects of the work.

Ethics Approval and Consent to Participate

This study was conducted in accordance with the guidelines of the Declaration of Helsinki and was approved by by the Ethics Committee of Beijing Chao-Yang Hospital, Capital Medical University (Approval No. 2020-Science-279). All experimental protocols were conducted in accordance with the relevant guidelines and regulations. Informed consent was obtained from all participants before sample collection.

Acknowledgment

The authors would like to thank all the staff and participants involved in this study for their contributions and cooperation. We are also grateful to the members of laboratory for their technical assistance and valuable discussions during the preparation of this manuscript.

Funding

This work was supported by the Beijing Municipal Administration of Hospitals Incubating Program (No.PX2023011); Beijing Chaoyang Hospital Science and Technology Innovation Fund (No.22kcjjzd-2); Beijing Natural Science Foundation (No.7254358).

Conflict of Interest

The authors declare no conflict of interest.

Supplementary Material

Supplementary material associated with this article can be found, in the online version, at https://doi.org/10.31083/CEOG48062.

References

[1] Gellersen B, Brosens IA, Brosens JJ. Decidualization of the human endometrium: mechanisms, functions, and clinical perspectives. Seminars in Reproductive Medicine. 2007; 25: 445–453. https://doi.org/10.1055/s-2007-991042.

[2] Ng SW, Norwitz GA, Pavlicev M, Tilburgs T, Simón C, Norwitz ER. Endometrial decidualization: The primary driver of pregnancy health. International Journal of Molecular Sciences. 2020; 21: 4092. https://doi.org/10.3390/ijms21114092.

[3] Tong J, Lv S, Yang J, Li H, Li W, Zhang C. Decidualization and Related Pregnancy Complications. Maternal-Fetal Medicine. 2022; 4: 24–35. https://doi.org/10.1097/FM9.0000000000000135.

[4] Deryabin PI, Borodkina AV. Stromal cell senescence contributes to impaired endometrial decidualization and defective interaction with trophoblast cells. Human Reproduction. 2022; 37: 1505–1524. https://doi.org/10.1093/humrep/deac112.

[5] Matsuyama S, Whiteside S, Li SY. Implantation and Decidualization in PCOS: Unraveling the Complexities of Pregnancy.

International Journal of Molecular Sciences. 2024; 25: 1203. https://doi.org/10.3390/ijms25021203.

[6] Verdin E. NAD^+ in aging, metabolism, and neurodegeneration. Science (New York, N.Y.). 2015; 350: 1208–1213. https://doi.org/10.1126/science.aac4854.

[7] Imai SI, Guarente L. NAD+ and sirtuins in aging and disease. Trends in Cell Biology. 2014; 24: 464–471. https://doi.org/10.1016/j.tcb.2014.04.002.

[8] Zhao Y, Lu Y, Zhang Y, Sun J, Li W, Cai L, *et al*. NAD+ Metabolism Maintains the Homeostasis of Decidual Macrophages in Early Pregnancy. The FASEB Journal. 2025; 39: e70674. https://doi.org/10.1096/fj.202500462R.

[9] Covarrubias AJ, Perrone R, Grozio A, Verdin E. NAD+ metabolism and its roles in cellular processes during ageing. Nature Reviews. Molecular Cell Biology. 2021; 22: 119–141. https://doi.org/10.1038/s41580-020-00313-x.

[10] Han S, Liu S, Jin NQ, Lv YS, Yang M, Ma S, *et al*. Mitochondrial energy metabolism is downregulated in repeated implantation failure patients related to alteration of PGC-1α acetylation level. Molecular Reproduction and Development. 2023; 90: 397–405. https://doi.org/10.1002/mrd.23691.

[11] Apostolov A, Naydenov M, Kalinina A, Nikolova M, Saare M, Aleksejeva E, *et al*. Endometrial Proliferative Phase-Centered View of Transcriptome Dynamics across the Menstrual Cycle. International Journal of Molecular Sciences. 2024; 25: 5320. https://doi.org/10.3390/ijms25105320.

[12] Mortazavi A, Williams BA, McCue K, Schaeffer L, Wold B. Mapping and quantifying mammalian transcriptomes by RNA-Seq. Nature Methods. 2008; 5: 621–628. https://doi.org/10.1038/nmeth.1226.

[13] Love MI, Huber W, Anders S. Moderated estimation of fold change and dispersion for RNA-seq data with DESeq2. Genome Biology. 2014; 15: 550. https://doi.org/10.1186/s13059-014-0550-8.

[14] Livak KJ, Schmittgen TD. Analysis of relative gene expression data using real-time quantitative PCR and the 2(-Delta Delta C(T)) Method. Methods (San Diego, Calif.). 2001; 25: 402–408. https://doi.org/10.1006/meth.2001.1262.

[15] Tang Y, Chen K, Song B, Ma J, Wu X, Xu Q, *et al*. m6A-Atlas: a comprehensive knowledgebase for unraveling the N6-methyladenosine (m6A) epitranscriptome. Nucleic Acids Research. 2021; 49: D134–D143. https://doi.org/10.1093/nar/gkaa692.

[16] Moiseeva TN, Bakkenist CJ. Regulation of the initiation of DNA replication in human cells. DNA Repair. 2018; 72: 99–106. https://doi.org/10.1016/j.dnarep.2018.09.003.

[17] Prigione A, Adjaye J. Modulation of mitochondrial biogenesis and bioenergetic metabolism upon in vitro and in vivo differentiation of human ES and iPS cells. The International Journal of Developmental Biology. 2010; 54 (11-12): 1729–1741. https://doi.org/10.1387/ijdb.103198ap.

[18] Fernandez-Marcos PJ, Auwerx J. Regulation of PGC-1α, a nodal regulator of mitochondrial biogenesis. The American Journal of Clinical Nutrition. 2011; 93: 884S–890S. https://doi.org/10.3945/ajcn.110.001917.

[19] Tamura I, Miyamoto K, Hatanaka C, Shiroshita A, Fujimura T, Shirafuta Y, *et al*. Nuclear actin assembly is an integral part of decidualization in human endometrial stromal cells. Communications Biology. 2024; 7: 830. https://doi.org/10.1038/s42003-024-06492-z.

[20] Liu S, Liao S, He J, Zhou Y, He Q. IGF2BP2: an m6A reader that affects cellular function and disease progression. Cellular & Molecular Biology Letters. 2025; 30: 43. https://doi.org/10.1186/s11658-025-00723-9.